Grafting of 2,8-dithia-5-aza-2,6-pyridinophane macrocycle on SBA-15 mesoporous silica for removal of Cu^{2+} and Cd^{2+} ions from aqueous solutions: synthesis, adsorption, and complex stability studies

Giulia Rossella Delpiano[1], Alessandra Garau[1], Vito Lippolis[1], Joanna Izabela Lachowicz[2,] and Andrea Salis[1,3,*]*

[1]*University of Cagliari, Department of Chemical and Geological Science, Cittadella Universitaria, 09042 Monserrato-Cagliari, Italy*

[2]*University of Cagliari, Department of Medical Sciences and Public Health, Cittadella Universitaria, 09042 Monserrato-Cagliari, Italy*

[3] *Consorzio Interuniversitario per lo Sviluppo dei Sistemi a Grande Interfase (CSGI), via della Lastruccia 3, 50019, Sesto Fiorentino (FI), Italy.*

Abstract

Silica-based mesoporous materials have received growing attention in the metal recovery from industrial processes although, in general, the adsorption of metal ions by silanols is rather poor. Nevertheless, a great improvement of metal ions removal from aqueous solutions can be achieved by grafting metal-chelators on the particles' surface. Combining metal-chelating properties of organic ligands, with high surface area of mesoporous silica particles make these hybrid nanostructured materials a new horizon in metal recovery, sensing and controlled storage of metal ions in industrial and mining processes. Here, the 2,8-dithia-5-aza-2,6-pyridinophane (L) macrocycle was grafted on SBA-15 mesoporous silica to obtain SBA-L mesoporous adsorbent for the removal and controlled recovery of Cd^{2+} and Cu^{2+} ions from aqueous solution in a broad pH range (4–11). By grafting about 0.3 mmol/g of L on SBA-15 a maximum loading capacity of 20.9 mg/g and 31.8 mg/g was obtained for Cu^{2+} and Cd^{2+}, respectively. The adsorption kinetics can be described with the pseudo-second order model while the adsorption isotherm (298 K) followed the Langmuir model. The latter, together with potentiometric studies suggests that the adsorption mechanism is based on metal chelation by the grafted macrocycle. In summary, SBA-L is an effective copper (II) and cadmium (II) chelator for possible applications where metal removal, storage and recovery are of basic importance.

Keywords

Functionalized ordered mesoporous silica; azathiamacrocycles; metal complexes; potentiometry, speciation diagrams, adsorption isotherm

Introduction

Heavy metals and their ionic forms can be toxic for the environment and living organisms even at very low concentrations.[1] For this reason, their uncontrolled release in the soil or surface waters should be avoided. Industry and mining are the main sources of metal contamination, particularly of water-soluble metal ions. Once in water, metal ions can be easily assumed by living organisms, thus interfering with their biological processes. Moreover, the accumulation in the human organism of heavy metal ions has been recognized as the source of several diseases.[2] The expansion of new metal-based technologies, for instance electronics for Information Technology (IT), mining and processing of metal ions worldwide,[3] is increasing the risks deriving from heavy metal pollution. In addition, the rapid development of industrial processes gives rise to the obtainment of new types of contaminating wastes for which conventional purification treatments (such as coagulation, precipitation, filtration, and others) are not always effective. To limit and possibly solve these issues fast, effective, and economic methods for metal ions removal from the environment are needed. Moreover, once recovered, metal ions should be reused according to the principles of the circular economy.[4-6] Over the years, several materials have been considered for metal ions recovery.[7-9] In particular, ordered mesoporous silicas (OMS) have high surface areas, tuneable pore sizes, low toxicity and can be easily functionalized. Among several applications in the field of heterogeneous catalysis[10] and biocatalysis,[11] functionalized OMS have been used as adsorbents for the effective removal of numerous organic pollutants[12] as well as metal ions.[13-15]

Grafting metal-chelating ligands on OMS surface is a promising way for obtaining effective metal ion adsorbents,[16-18] with the possibility of metal recovery by changing experimental conditions (e.g. pH). Moreover, functionalized OMS are a new frontier in selective metal sensing, and some examples of effective silica-modified electrodes for electrochemical detection of organic pollutants and metal ions have been recently reported.[19-21]

Among hundreds of known metal-chelating molecules, macrocyclic ligands are particularly interesting due to their ability to bind alkaline earth, transition (particularly heavy) metals both in water and organic solvents by changing their molecular structure and the nature of donor atoms.[22-24] The ligand-metal binding property is mainly provided by the presence of electron-donor atoms with appropriate soft-hard properties, while metal selectivity can be modulated by the macrocycle ring size and conformational properties.[22] Aromatic rings, often introduced into the macrocyclic structure to provide a structurally rigid moiety, are also important moieties for the coordination of metal ions especially within small-sized macrocyclic polyamine systems.[25] For instance, Blake et al.[26] studied extensively the coordination properties towards “borderline” and “soft” metal ions (e.g. Cu^{2+}, Zn^{2+},

Cd^{2+}, Hg^{2+}, and Pb^{2+}) of the pyridine based, N_2S_2-donating 12-membered macrocycle 2,8-dithia-5-aza-2,6-pyridinophane (hereafter referred also as **L**). Their results showed that L forms very stable 1:1 complexes with Cu^{2+} and Hg^{2+}, and displays a higher binding ability for Cd^{2+} and Pb^{2+} with respect to Zn^{2+}, due to the presence of the soft S-donors.

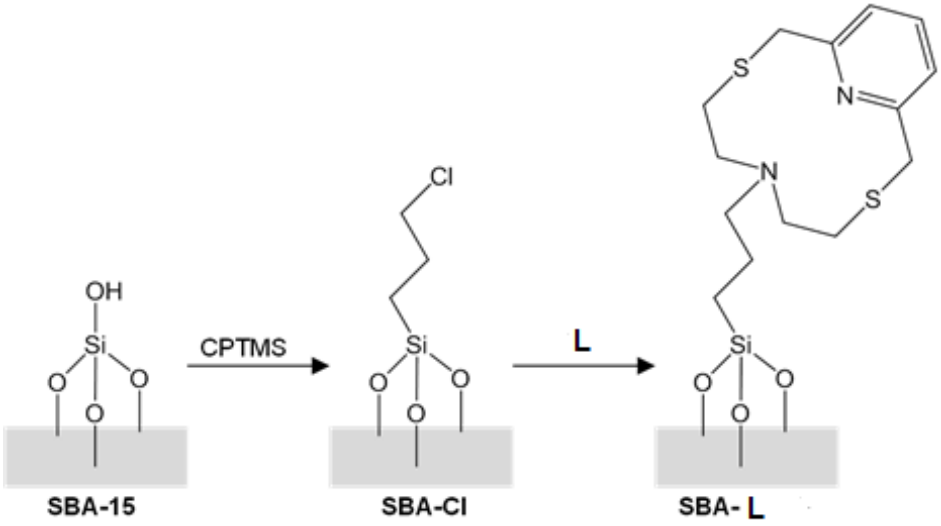

Scheme 1. Schematic representation of 2,8-dithia-5-aza-2,6-pyridinophane (L) ligand grafting on SBA-15 mesoporous material. CPTMS = (3-chloropropyl)trimethoxysilane,

Here the macrocycle L, which is an effective metal chelator but with low water solubility, was grafted on SBA-15 to give SBA-L adsorbent according to Scheme 1. The aim of this work was to join the metal chelating ability of a macrocycle ligand with the vehicle properties of mesoporous silica, which has large surface area and wide pores to allow macrocycle molecules grafting in the inner surface. The copper (II) and cadmium (II) chelating ability of SBA-L toward Cu^{2+} and Cd^{2+} was determined by means of potentiometric studies, as well as by determining the adsorption kinetics and isotherms. The SBA-L adsorbent could be reused, and the chelated metal ions were efficiently recovered.

Experimental Section

Chemicals. Pluronic copolymer P123 (EO20PO70EO20) tetraethylorthosilicate, TEOS (≥99%); (3-chloropropyl)trimethoxysilane, CPTMS (≥97%); copper(II) chloride dihydrate, $CuCl_2 \cdot 2H_2O$ (≥99.0%), cadmium(II) chloride $CdCl_2$ (≥99.0%), toluene (≥99.7%), dimethylformamide (DMF, ≥99.9%), anhydrous acetaldehyde (>99%), diethyl ether (99.8%), acetone (≥99%), HCl (37%), NaCl, NaOH pellets, ammonium hydroxide, citric acid, oxalyldihydrazide (>98%), Ethylenediaminetetraacetic acid (EDTA) were purchased from Sigma-Aldrich (Milano, Italy). Ethanol (99.8%) was purchased from Honeywell. Acetonitrile (MeCN) was distilled over CaH_2.

Copper(II) and Cadmium(II) stock Normex solutions (1000 ppm in HNO_3 2% m/m) were Carlo Erba products.

A previously described method was used in the preparation of 0.1 M carbonate free KOH solution.[27] L and SBA-L solutions were acidified with stoichiometric equivalents of HCl. Metal solutions were prepared by dissolving the required amount of metal salt in pure double distilled water, to which a stoichiometric amount of HCl was previously added to prevent hydrolysis. These solutions were standardized by the complexometric method with EDTA and proper indicators.

Synthesis of L, SBA-15 and SBA-L. 2,8-dithia-5-aza-2,6-pyridinophane (L) was prepared according to the previously described procedure and the qualitative analysis confirmed the purity of the ligand.[26] The synthesis of SBA-15 mesoporous silica and its functionalization with (3-chloropropyl)trimethoxysilane (CPTMS) were performed according to our previous work.[28] Then, a mass of 100 mg of SBA-Cl was dispersed in 25 mL of anhydrous acetonitrile, with 93 mg of K_2CO_3 and 40 mg of L. The resulting suspension was kept under stirring at 90°C for 48h under nitrogen atmosphere. SBA-L was collected by filtration, washed with acetonitrile, dichloromethane, and water, and dried under vacuum overnight. The liquid phase was treated to recover the unreacted L.

Physico–Chemical Characterizations. The structural characterization of SBA-15 was performed by small-angle X-rays scattering (SAXS) and Transmission Electron Microscopy (TEM) analysis. SAXS patterns were recorded with a S3-MICRO SWAX camera system (Hecus X-ray System, Graz, Austria). CuKα radiation of wavelength 1.542Å was provided by a Genix X-ray generator, operating at 30 kV and 0.4 mA. TEM analysis was performed with a Jeol JEM 1400 Plus, operating at 120 kV. The textural parameters of the materials such as the surface area (Brunauer-Emmett-Teller, B.E.T.) and pore size distribution (Barrett-Joyner-Halenda, B.J.H.) were determined by N_2 adsorption/desorption isotherms at 77 K carried out on an ASAP 2020 instrument. FTIR spectroscopy was carried out through a Bruker Tensor 27 spectrophotometer equipped with a diamond-ATR accessory and a DTGS detector. A number of 128 scans with a resolution of 2 cm^{-1} were averaged in the spectral range 4000–400cm^{-1}. Thermogravimetric Analysis (TGA) was performed using a STA6000 - Perkin Elmer in the 25–850°C range, under oxygen flow (heating rate = 10°C/min; flow rate = 40 mL min^{-1}).

Quantitative analysis of Cd^{2+} and Cu^{2+} concentrations in water. Cd^{2+} and Cu^{2+} concentrations in aqueous solutions were analysed by inductively coupled plasma optical emission spectroscopy (ICP-OES). The operational parameters were as follows: RF Power: 1.2 kW, Plasma gas: 12 L min^{-1}, Aux gas: 1.0 L min^{-1}, Nebulizer flow: 0.7 L min^{-1}, Emission lines (nm): Cd (214.439, 226.502 and 228.802); Cu (213.598, 324.754 and 327.395); Ar (419.832 and 737.212) was used as internal standard. No spectral interference was observed. The standard solutions ranging from 0.01 to 300 mg/L in 1% nitric acid were prepared by the analytical dilution of Normex standard cadmium(II) solutions. The limit of detection (LOD) was determined at 0.05 mg/L. Moreover, the Cu^{2+} concentrations in aqueous solutions during the kinetic and adsorption studies were analysed through a colorimetric method.[29] Briefly, the coloured adduct of Cu^{2+} with oxalyldihydrazide was formed at pH = 9 upon mixing Cu^{2+} solution with citric acid, ammonium hydroxide, acetaldehyde and oxalyldihydrazide. The absorbance of the solutions was measured at 540 nm after 30 min incubation in the dark.

Determination of adsorption kinetics and isotherms- The adsorption kinetics of Cu^{2+} or Cd^{2+} on SBA-L were carried out by suspending 15 mg of mesoporous adsorbent in 10 mL of 5 mg L^{-1} (for copper(II)) and 3.5 mg L^{-1} (for cadmium(II)) of metal solution for time intervals ranging from 2 min to 24 h at pH = 5 (for copper(II) solutions) and pH = 7 (for cadmium(II) solutions). All samples were kept under rotation (22 rpm) at 298 K. The process was then stopped, and the solution was filtered through Ø 0.2 μm syringe cellulose filter (Minisart Syringe Filter). For the isotherm studies, mesoporous materials were treated with metal ion solutions of variable concentration, ranging from 0.5 to 300 mg L^{-1}; the reactions were stopped after 5h. The residual copper(II) and cadmium(II) concentrations in the water solution after adsorption on SBA-L were quantified by Vis-spectrometry (upon colorimetric method) and ICP-OES, respectively. Each experiment was carried out at least in triplicate.

The adsorption kinetics was quantified by measuring the decrease of metal ion (either copper(II) or cadmium(II)) concentration in the adsorbing solution, at given times. The adsorption isotherms were determined by plotting the adsorbed amount (q_t) of Cu^{2+} and Cd^{2+} (mg g^{-1}) versus the equilibrium concentration (C_{eq}) of Cu^{2+} and Cd^{2+} (mg L^{-1}) in the adsorbing solution. The kinetic and isotherm experimental data were fitted through three different isotherm and kinetic models described previously.[28]

Potentiometric and spectrophotometric measurements. Protonation and complex-formation equilibrium studies were carried out in 0.1 M NaCl at 298.1±0.1 K using an automatic Metrohm

titrator under the same conditions previously described.[16] The OMS (SBA-15 and SBA-L) samples were stored at 50 °C and cooled in a desiccator to room temperature before being weighed (analytical weight scale, precision ± 0.01 mg). The combined Metrohm electrode was calibrated as a hydrogen-ion activity probe by titrating previously standardized amounts of HCl with CO_2-free NaOH solutions and determining the equivalence point by Gran's method,[24] which gave the standard potential, E°, and the ionic product of water (pK_w = 13.74(1) in 0.1 m NaCl at 298.1 K). The computer program HYPERQUAD2013.[25] and Hyss software[30] were used to calculate ligand content (in mmol) in MMs material, MMs-ligand protonation, and complex stability constants from potentiometric data.

The potentiometric titrations were prepared from acidic to alkaline conditions (the studied pH range 2.5–11.0). Solutions at 0.1 M ionic strength in NaCl were titrated at 25.0 °C with 0.1 M NaOH. An mV signal drift module was used to reach equilibrium after each base addition (base volume for each addition 10 μL) and obtain optimal accuracy of measurements. The working OMS content was 3.0–3.1 mg in 20 mL of water. The operating ligand concentration was 3.7×10^{-4} (free L) and 4.5×10^{-5} (for L grafted on SBA-15; SBA-L). The studies of complex formation were carried using constant ligand concentration, and 1:1, 1:2, and 1:5 metal/ligand molar ratios. Each measurement, both for ligand protonation and metal-complex formation experiments, was carried out at least three times to verify the repeatability. The different titration curves were calculated as separated curves without significant variations in the values of the calculated stability constants. Finally, the sets of data were merged and treated simultaneously to give the final stability constants. Different equilibrium models for the complex systems were generated by eliminating and introducing different species. Only those models for which the HYPERQUAD program furnished a variance of the residuals $\sigma^2 \leq 9$ were considered acceptable. Such a condition was unambiguously met by a single model for each system. The UV-Vis measurements were carried with Varian Cary 60 spectrophotometer. The pH combined glass electrode was daily calibrated with buffer solutions (pH = 4.00, pH = 7.00, pH = 9.00 Mettler Toledo).

SBA-L reuse and metal ions recovery. In order to study the reuse of the adsorbent material and the recovery of chelated metal ions , 7 mg of SBA-L were suspended in a solution containing 10 ppm of copper(II) and 10 ppm of cadmium(II) ions (pH = 5; the pH value of the solution was directly adjusted using concentrated HCl/NaOH at each experimental point) and kept under stirring for 6 h. Successively, the samples were centrifuged (12,000 rpm; 30 min) to separate SBA-L from metal ions solution, which was analysed through ICP-OES for the quantitative determination of metal ion concentrations. Instead, the SBA-L-metal ion sample was used for the desorption experiment by

suspending in 1 mL of EDTA-2Na solution (0.02 mol L^{-1}; pH = 7) under stirring for 24 h. Then, the samples were centrifuged (12,000 rpm; 30 min) to separate SBA-L solid from EDTA solution. The latter was analysed through ICP-OES for the quantitative determination of metal ion concentrations. The adsorption/desorption cycle was repeated 4 times with three independent samples.

Results and Discussion

Physico–Chemical Characterizations of SBA-15 and SBA-L. The structural characterization of SBA-15 was carried out by using a transmission electron microscopy (TEM) and a small angle X-rays scattering (SAXS) analyses. TEM images in Figure 1 clearly show the occurrence of parallel channels forming a hexagonal array of mesopores. The SAXS plot in Figure 2A has the typical pattern of 2D hexagonal phases. It consists of an intense peak relative to the reflections of the planes 10, and two less intense peaks due to planes 11 and 20, with a resulting lattice parameter of 116.8 Å (Table 1).

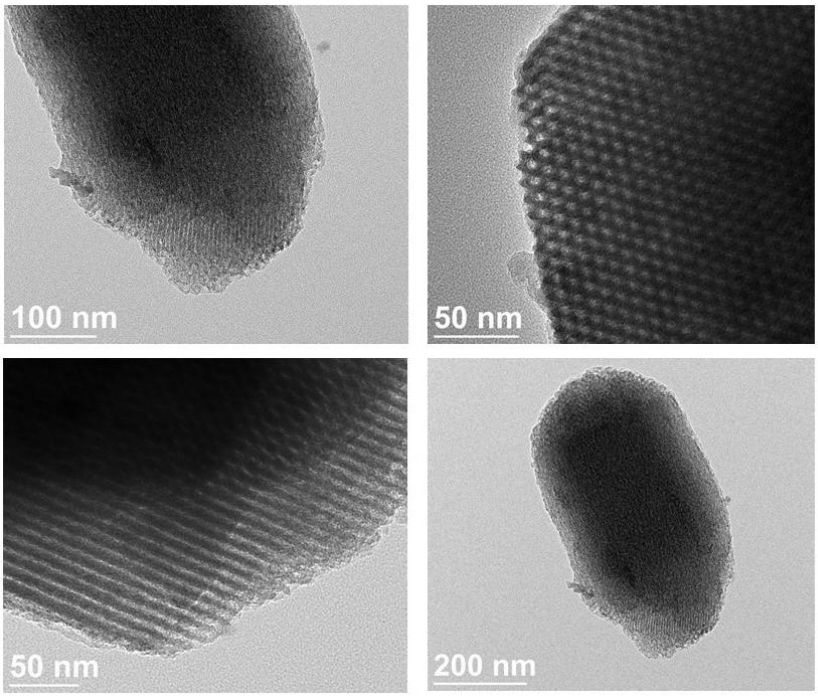

Figure 1. TEM micrographs of SBA-15. Bar = 50 nm, 100 nm and 200 nm.

The textural characterization of the samples was carried out through N_2 adsorption/desorption isotherms at 77 K (Figure 2B) resulting in a surface area of 692 m^2g^{-1} (Table 1). A hysteresis cycle due to the capillary condensation confirms the mesoporosity of the SBA-15 sample. The pore size distribution, obtained by applying the BJH method[31] to the desorption branch of the isotherm, has a maximum at 66 Å (Table 1). SBA-15 functionalization results in a decrease of surface area and pore

size being, S_{BET} = 372 m^2g^{-1}, d_p = 58 Å and S_{BET} = 255 m^2g^{-1}, d_p = 47 Å for SBA-Cl and SBA-L, respectively (Table 1). The decrease of surface area and pore size confirms the successful grafting of L in the internal pores' surface. However, it is very likely that L is also grafted on the external surface of SBA-15 particles.

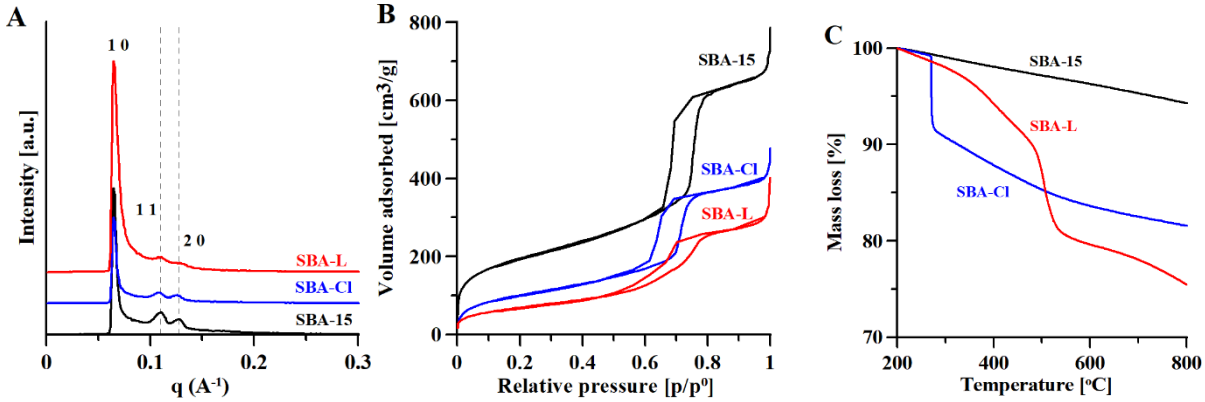

Figure 2. Characterization of SBA-15, SBA-Cl and SBA-L mesoporous silica. A) SAXS patterns. B) N_2-adsorption/desorption isotherms. C) Thermal analysis.

Thermogravimetric analysis (TGA) was used to characterize the functionalized SBA-15 (Figure 2C) and evaluate organic functionalization inside the pores. The mass loss (%) as a function of the temperature (°C) of SBA-15, SBA-Cl (19 %) and SBA-L (26%) samples confirms the successful functionalization of SBA-15 with both CPTMS and L macrocycle (Figure 2C). TGA also allowed estimating the amount of L ligand grafted on SBA-15 which was 70 mg/g (Table 1).

Table 1. Characterization of original and functionalized SBA-15 samples.

Sample	[a]S_{BET} (m^2 g^{-1})	[b]d_p (Å)	[c]*a* (Å)	Mass loss (%)	Loading (mg/g)	Loading (mol/g)
SBA-15	692	66	116.8	6	-	
SBA-Cl	372	58	115.8	19	130	1.68×10^{-3}
SBA-L	255	47	114.1	26	70	0.291×10^{-3}

[a]Surface area calculated by the BET method; [b]Pore diameter calculated by applying the BJH method to the isotherm desorption branch; [c]Lattice parameter obtained by SAXS $a = 2\cdot d/(3)^{0.5}\cdot(h^2+k^2+hk)^{0.5}$

Adsorption kinetics and isotherms. The adsorption of Cu^{2+} and Cd^{2+} ions on SBA-L from aqueous solution was then studied. The pH for the adsorption kinetics and isotherms experiments was chosen on the basis of metal hydrolysis speciation plots[32] and metal-complex formation stability constants on the SBA-L surface (see above). It was essential to work at a pH where the metal-complex formation is at 100% and, at the same time, there is neither metal hydrolysis nor precipitation. For these reasons, Cu^{2+} adsorption was carried out at pH = 5 where the species $[Cu(SBA(SiO)(L))]^+$ is prevalent, while pH = 7 was chosen for Cd^{2+} where the $[Cd(SBA(SiO)(L))]^+$ species is predominant (see above). Figure 3A shows the adsorption kinetics of Cu^{2+} and Cd^{2+} on SBA-L. The adsorbed amount (q_t) increases when the contact time (t) increases, until a constant value (q_e), corresponding to the adsorption equilibrium, is reached. Both cations reach the adsorption equilibrium after about 30 min. Under these conditions, the q_e of Cd^{2+} on SBA-L was 24 mg/g (0.2 mmol/g), while that of Cu^{2+} was q_e = 3.5 mg/g (0.055 mmol/g). Three different kinetic models - namely, pseudo-first order, pseudo-second order, and intraparticle diffusion model - were tested as shown in Figure 3B-D. The fitting of the experimental data using the pseudo-first order gave low correlation coefficients (Table 2), thus, suggesting the inadequacy of this model to describe both Cu^{2+} and Cd^{2+} adsorption on SBA-L. On the contrary, the pseudo-second order model resulted in a very good fitting, as demonstrated by the high correlation coefficients ($R^2 > 0.99$). The values of q_e calculated from pseudo-second order model are 3.57 mg/g for Cu^{2+} and 23.8 mg/g for Cd^{2+}. The good fitting of the adsorption data obtained by the pseudo-second order model suggests that the adsorption of the metal ions on the adsorbent sites is the rate determining step.[33] The fit of the intraparticle diffusion model (Figure 3D) is of lower quality than that of the pseudo-second order model, thus supporting the goodness of the latter which gives the best description of the kinetic data.

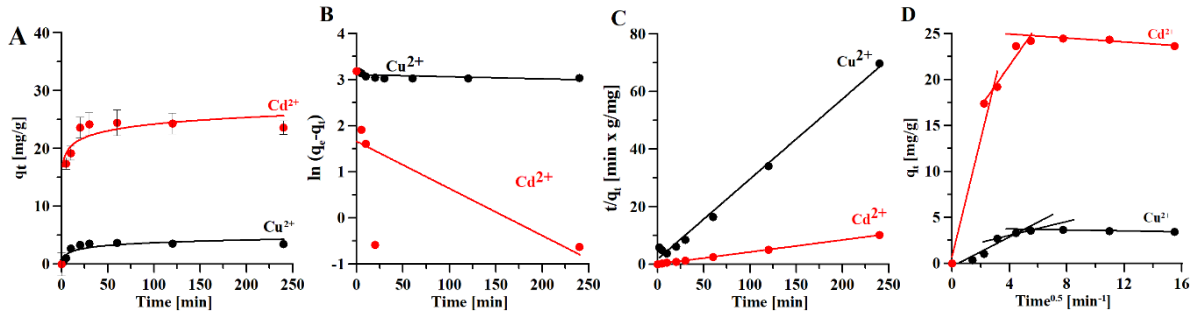

Figure 3. Adsorption kinetics of Cu^{2+} (black) and Cd^{2+} (red) on SBA-L. A) Adsorbed amount q_t versus time. B) Pseudo-first order model; C) Pseudo-second order model; D) Intraparticle diffusion model. For Cu^{2+} kinetics studies: Initial metal ion concentration = 5 ppm; pH = 5; stirring speed = 22 rpm; T = 298 K. For Cd^{2+} kinetics studies: Initial metal ion concentration = 3.5 ppm; pH = 7; stirring speed = 22 rpm; T = 298 K.

Table 2. Comparison among kinetic models for Cu^{2+} and Cd^{2+} adsorption on SBA-L.

	[a]Pseudo First Order			[b]Pseudo Second Order			[c]Intraparticle Diffusion		
Ion	k' **(1/min)**	$q_{e\ cal}$ **(mg/g)**	R^2	k'' **(g/mg·min)**	$q_{e\ cal}$ **(mg/g)**	R^2	k_i **(g·mg^{-1}min$^{-0,5}$**	x_i **(mg/g)**	R^2
Cu^{2+}	5×10^{-4}	22.28	0.2874	0.06	3.57	0.9927	0.81	−0.362	0.8297
							0.38	1.52	0.9688
							−0.03	3.82	0.9441
Cd^{2+}	1×10^{-2}	3.61	0.3464	0.16	23.81	0.9996	6.39	0.71	0.9591
							2.22	12.62	0.8888
							−0.11	25.36	0.9322

[a]Pseudo-First Order linearized equation[34]: $\ln(q_e - q_t) = lnq_e - k't$; where k' is the pseudo-first order constant; [b]Pseudo-Second Order linearized equation[34] $\frac{t}{q_t} = \frac{1}{k'' \cdot q_e^2} + \frac{t}{q_e}$; where k'' is the pseudo-second order constant; [c]Intraparticle diffusion model linearized equation[34] $q_t = k_i \cdot t^{0.5} + x_i$; where ki is the intraparticle diffusion constant.

The adsorption isotherms (Figure 4) show that the maximum adsorbed amount of metal ions, corresponding to the plateaus, are 20.9 mg/g (0.329 mmol/g) for Cu^{2+} and 31.8 mg/g (0.284 mmol/g) for Cd^{2+} (Table 4). The shape of the isotherms is consistent with Langmuir model which considers the formation of a monolayer of adsorbate on the adsorbent's surface. This is consistent with the formation of a metal/L complex at 1:1 molar ratio since, as reported in Table 1, L loading in SBA-L is 0.291 mmol/g as determined through TG analysis.

The Gibbs free Energy (ΔG^0) for the adsorption process (Table 3) was calculated according to the equitation: $\Delta G^0 = -RTlnK_e^0$, where R is the universal gas constant (8.314 $J \cdot K^{-1} \cdot mol^{-1}$), T is the absolute temperature (298 K) and K_e^0 is the thermodynamic equilibrium constant, calculated by means of the equation:[35]

$$K_e^0 = \frac{K_L \cdot 1000 \cdot MM_{Adsorbate} \cdot [Adsorbate]^0}{\gamma}$$

where K_L is the Langumir constant (L/mg), $MM_{Adsorbate}$ is the molar mass of the adsorbate (g/mol), $[Adsorbate]^0$ is the standard concentration of the adsorbate (1 mol/L) and γ is the activity coefficient (dimensionless).[35] As reported in Table 3, the ΔG^0 was negative for both adsorption processes, more

precisely −25.5 kJ/mol and −33.7 kJ/mol for Cu^{2+} and Cd^{2+}, respectively. These data confirm the spontaneous nature of the adsorption process.

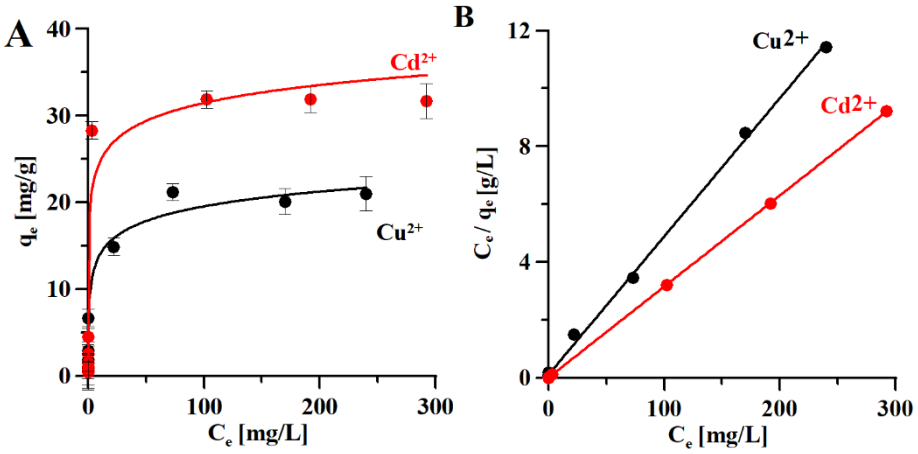

Figure 4. Adsorption isotherm of Cu^{2+} and Cd^{2+} on SBA-L A). Adsorption data were fitted using linearized Langmuir isotherms B). Adsorption experiments were carried out for 24 h at pH = 5 (for copper(II)) and pH = 7 (for cadmium(II)) and T = 298 K.

Table 3. Langmuir adsorption isotherm parameters for Cu^{2+} and Cd^{2+} on SBA-L.

Ion	pH	Langmuir					
		[a]K_L (L/mg)	[b]q_M (mg/g)	q_M (mmol/g)	R^2	$K_e°$	$\Delta G°$ (kJ/mol)
Cu^{2+}	5.0	0.468	20.9	0.329	0.999	2.97×10^4	−25.5
Cd^{2+}	7.0	7.16	31.8	0.284	1	8.05×10^5	−33.7

[a]Langmuir constant and [b]maximum monolayer coverage capacity obtained by the linearized form of the Langmuir isotherm model equation $\frac{C_e}{q_e} = \frac{1}{K_L \cdot q_M} + \frac{1}{q_M} C_e$.[36]

Protonation and metal-complex equilibria. The stability in aqueous solutions, the equilibrium formation constant, the solubility, and other properties of macrocycle-metal ion complexes depend on different factors, namely the nature of the metal ion, the structure of the ligand and the composition of the complex. The most important metal ion-related factors are the oxidation state, the ion size, and the electron shell structure. Factors related to the ligand are the flexibility, the charge, the nature and number of donor sites, and the molecular structure.[22] The combination of all these factors makes

difficult the exact prediction of the ligand/metal complex-stability. However, experimental data from previous works can provide some hints.[37] Generally, aliphatic azamacrocycles form stable and inert complexes (i.e., complexes that decompose slowly under the action of external factors or competing ligands) with metal ions even in very acidic solutions. Nevertheless, the practical application of the complexes is limited by slow complexation kinetics.[22] The stability of metal/aliphatic ligands complexes is strongly influenced by entropy. Free aliphatic macrocyclic ligands occur in solution as a mixture of several conformers in dynamic equilibrium. The formation of metal-complexes brings to the loss of some of their degrees of freedom, thus the entropy decreases (even if the total entropy - system and environment - increases due to the release of water molecules from the metal ion-hydration shell). Conversely, structurally rigid macrocyclic ligands do not appreciably change the conformation after the formation of the metal complex therefore, the entropy of the system increases less than in the case of aliphatic macrocyclic ligands, which are thermodynamically more favourable.[37] In addition, a rigid macrocyclic structure can force a particular coordination geometry to the metal centre, while open-chain chelators are more easily adaptable to the coordination characteristics of the metal centre.[38] For this reason, an increase in the ligand rigidity could increase the binding selectivity toward specific cations.[39] Blake et al.[26] investigated L ligand coordination mode and complex stability with Cu^{2+}, Zn^{2+}, Cd^{2+}, Hg^{2+}, and Pb^{2+} ions by the means of potentiometry (water solution, I = 0.1 M NMe_4NO_3, [L] = 1.0×10^{-3} M) and single crystal X-ray diffraction analysis. Metal complexation of L in aqueous solution generally occurs at acidic pH values to give $[ML]^{2+}$ species while hydroxo- complexes $[ML(OH)]^{+}$ form at alkaline pHs. The hydroxo-complexes of Zn^{2+}, Cd^{2+}, Hg^{2+} and Pb^{2+} precipitate at slightly alkaline pH thus preventing to carry out potentiometric studies. The stability of the formed complexes increases in the order $Zn^{2+} < Pb^{2+} < Cd^{2+} < Cu^{2+} < Hg^{2+}$. Noteworthily, Cu^{2+} and Hg^{2+} complexes are more stable than complexes with other known polyamine ligands. The lowest stability of the Zn^{2+} complexes, which is usually similar to that of Cd^{2+} and Pb^{2+} complexes with polyamine, could be explained by the presence of the soft S-donors, within the macrocyclic structure. In agreement with a general N > S donor affinity trend for the studied metal ions, and with a better binding ability of a pyridine nitrogen toward transition and post-transition divalent cations, the L ligand forms less stable complexes than its structural analogue containing only N-donors in the aliphatic portion of the ring,[40]and more stable complexes than [12]aneNS_2O (1-aza-4,10-dithia-7-oxacyclododecane).[41]

The aim of our studies was the determination of metal/ligand complex stoichiometry, metal binding sites and complex formation constants for the ligand grafted on the surface of SBA-L mesoporous material. To compare the metal/free ligand complex formation with the metal complexes formed on the surface of L-grafted mesoporous material, we performed potentiometric titrations of free and

grafted L ligand with metal ions under the same experimental conditions. Respect to Blake et al.,[26] we used lower ligand and metal concentrations in order to avoid precipitation of hydroxo-complexes. Moreover, we used UV-Vis spectroscopy to determine metal binding sites in water solution on changing pH conditions. Finally, FTIR spectroscopy was used to support the metal-binding mode of SBA-L in solid state.

Free ligand protonation and metal-complex equilibria. Potentiometric titrations (Figure 5) allowed to calculate one protonation constant of free L occurring at basic pH (Table 4) that can be assigned to the aliphatic nitrogen atom, rather than to the pyridine nitrogen, which is usually protonated at acidic pH.[42]

Table 4. Protonation constants (log *K*) of L, L grafted on SBA-15 and cumulative formation constants (log *β*) of $Cu^{2+}$and Cd^{2+} complexes with free L and L grafted on SBA-15 at 25 °C, 0.1 M NaCl ionic strength, calculated using the Hyperquad program[20] for potentiometric measurements. The constants for the Cu^{2+} and Cd^{2+} hydroxides at 25 °C and 0.1 M ionic strength, are taken from the literature.[32] ((*) Cumulative constant ($[ML]^{2+} + 2OH^- = [ML(OH)_2]$).

Formed Species	**Literature data (log *K*)[26]**	**Experimental data (log *K*)**		
	Free L	**Free L**	**Formed Species for functionalized OMS**	
$[LH]^+$	8.32(1)	8.73(2)	[SBA(SiOH)(L)]	9.48(5)
$[LH_2]^{2+}$	1.5 (1)	-	$[SBA(SiOH)(LH)]^+$	8.8(2)
	Literature data (log *K*)[26]	**Experimental data (log *β*)**		
$[CuL]^{2+}$	10.05(7)	9.54(6)		
$[CuL(OH)]^+$	6.09(4)	0.71(6)		
$[CuL(OH)_2]$	2.3(1)	-		
			$[Cu(SBA(SiO)(L))]^+$	21.4(7)
			[Cu(SBA(SiO)(L))(OH)]	14.6(5)
$[CdL]^{2+}$	9.12(2)	6.25(4)		
$[CdL(OH)_2]$	-	-11.0(5)*		
			$[Cd(SBA(SiO)(L))]^+$	19.0(1)
			$[Cd(SBA(SiO)(L))(OH)_4]^-$	-13.5(5)

The $[CuL]^{2+}$ complexes start forming already at very low pH values (Figure 5B). The formation of $[CuL(OH)]^{+}$ complex occurs above pH = 8 (Figure 5B) likely due to deprotonation of water molecule in the metal coordination sphere. The formation of the $[CdL]^{2+}$ 1:1 complex takes place from pH = 5, in our experimental conditions.

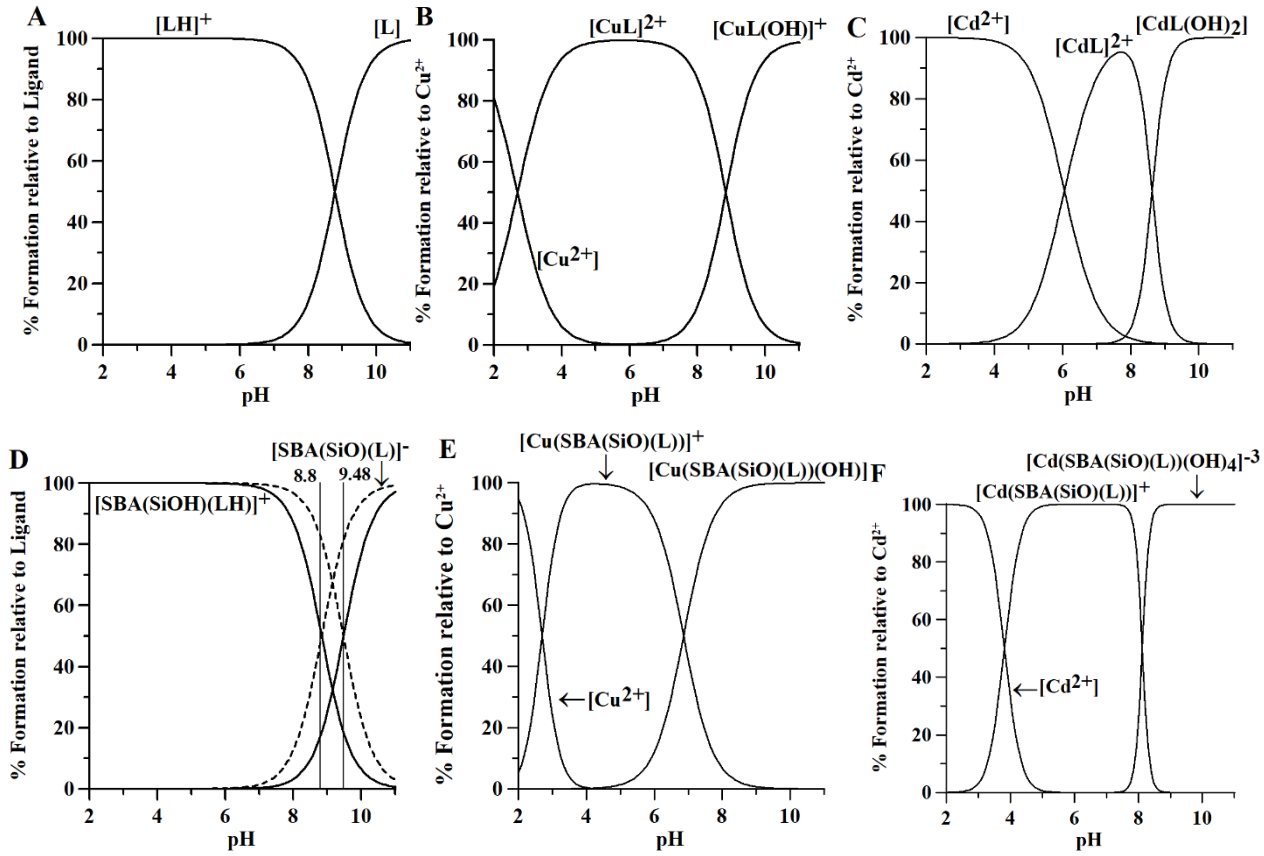

Figure 5. Speciation plot of free L (A) and grafted on SBA-15 (D)*. Distribution curves of (B) and (E) Cu^{2+}; (C) and (F) Cd^{2+} complexes with free L and grafted on SBA-15, respectively. Plots calculated on the base of stability constants (Table 5) with Hyss program.[30] (*) Dashed lines represents species deriving from a partial deprotonation of $[SBA(SiOH)(LH)]^{+}$ either of the silanol groups or the grafted $[LH]^{+}$ groups according to proper log *K* (Table 5) values.

The coordination mode in $[CuL](NO_3)_2$ complex was previously determined by X-ray crystallography using single crystals obtained from EtOH/MeCN (50:50 v/v) solution.[26] The central metal ion was coordinated by six donor atoms in the octahedral geometry, namely two N- and two S-donor atoms of the ligand, and two O- atoms from nitrate anions (Figure 6A). Here we analysed the complex structure in aqueous solution by the means of UV-Vis and FTIR spectroscopies. It can be observed in Figures 6B and 6C that at acidic pH the $[CuL]^{2+}$ complex is formed (green colour solution) and the characteristic d–d band with maximum at 730 nm can be assigned to the presence of nitrogen

atom(s) in the Cu^{2+} coordination core, while the band below 400 nm can be assign to S(σ)→Cu^{2+} charge transfer (LMCT).[43] The bands at high energy correspond to intramolecular π→π* and n→π* transitions[44]. When pH increases, the hypso- and hypochromic shift of the bands at 380 and 730 nm can be observed. Such changes could be due to a changing of the donor atom set in the metal coordination core. Remarkably, potentiometric studies showed a proton dissociation above pH = 8 (Figure 5B), which could be assigned to the dissociation of a water molecule. The Figure S1 presents the FTIR spectra of free L and the Cu^{2+}/L complex in the solid state. Upon the metal-complex formation, the slight shift of the bands in the 400–2000 cm^{-1} region, and the slight enlargement of the bands in the 1600–1700 cm^{-1} region can be observed. Significant changes can be observed in the region 2000–4000 cm^{-1}, where new bands in the region 3200–3600 cm^{-1} appear which could be associated to the presence of water molecules in the complex and relative intramolecular hydrogen bonds.

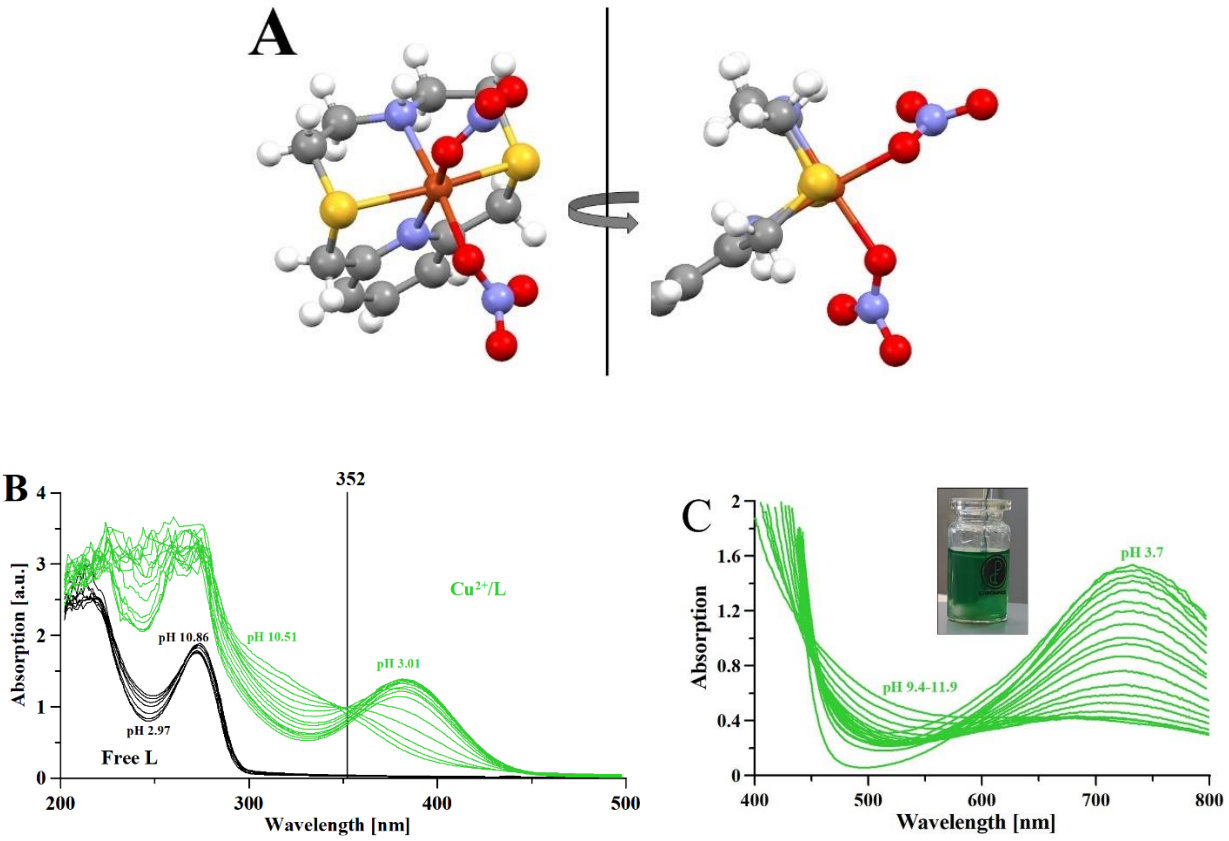

Figure 6. Characterization of the Cu^{2+}/L complex in solution and in the solid state. A) Crystal structure of $[CuL](NO_3)_2$ complex (CCDC n. 238263). Data available on https://www.ccdc.cam.ac.uk/structures/. UV-Vis spectrum of the Cu^{2+}/L (1:1 molar ratio) complex in MeCN/H_2O (50:50 v/v) solution B) 200–500 nm spectral range: $C_L = C_{Cu}^{2+}$ = 1 mM, l =1 cm, C) 500–800 nm spectral range: $C_L = C_{Cu}^{2+}$ = 10 mM, l = 1 cm.

As previously shown by Blake et al.[26], L forms complexes with Cd^{2+} ions. In our experimental conditions, the $[CdL]^{2+}$ complex forms above pH = 4 (Figure 5C) and remains stable even at basic pH, where the hydroxo complexes $[CdL(OH)]^{+}$, and $[CdL(OH)_2]$ are formed (only the cumulative formation constant for the latter was determined in the experimental conditions used), most likely due to the dissociation of a water molecule in the metal coordination core. The FTIR spectrum (Figure S2) of the Cd^{2+}/L complex is similar to that of the Cu^{2+} complex, suggesting the same coordination mode of the ligand, with only slight changes in the 3200 cm^{-1} region and higher intensity of the bands in the 3400–3600 cm^{-1} region.

SBA-L protonation and metal-complex equilibrium. In the next step, we investigated the metal coordination pattern on the L functionalized mesoporous material by the means of potentiometry and FTIR measurements. The potentiometric studies showed their great utility in the studies of functionalized OMS and their metal-complexes[16] and were used to establish the stoichiometry and stability of the formed complex on the SBA-L internal and external surface , and to some extent, can indicate the donor atoms in the metal coordination core. FTIR spectra (Figure S3) showed the changes in the spectroscopic bands, which can be assigned to the complex formation and indicate the donor atoms in the metal complex.

The potentiometric titration of functionalized OMS allowed to obtain the protonation constants and the precise ligand and dissociating silanol groups concentration on the OMS surface. The amount of L grafted on SBA-15 measured through potentiometric titrations was 0.3 mmol/g in agreement with the values obtained through TGA (Table 1). In addition, potentiometric data allowed us calculating the cumulative stability constants (Table 4) of the formed Cu^{2+} and Cd^{2+} complexes with L grafted on mesoporous silica.

In order to assign the protonation constants of L grafted on SBA-15 and dissociating silanol groups (SiOH), we introduce $[SBA(SiOH)(LH)]^{+}$ nomenclature to indicate the fully protonated functionalised OMS material. Previous studies under similar experimental conditions showed that silanol groups of SBA-15 had one protonation constant (log K = 10.0),[16] due to the dissociation of silanols (SiOH) into SiO^{-}. Grafting L on SBA-15 leads to two distinct protonation constants (Table 4), log K_1 = 8.8(2) for the aliphatic nitrogen of L and log K_2 = 9.48(5) for silanols (SiOH). Importantly, in our experimental conditions the molar ratio between silanols and nitrogens is equal to 3.2. Moreover, the slight differences in the pK values of free ligand, SBA-15 and the final

$[SBA(SiOH)(LH)]^+$ complex suggest the formation of intramolecular hydrogen bonds between nitrogen and oxygen atoms of silanols at different pHs.

As shown in our previous studies,[16] silanols of SBA-15 do not form stable complexes with metal ions, but can participate to the coordination shell of the metal ion in the presence of other ligands grafted on the OMS surface. In some cases, such co-participation can enhance the overall stability of the formed metal complex. Indeed, the cumulative formation constants of the Cu^{2+} and Cd^{2+} complexes with L grafted on SBA-15 are higher with respect to the complexes formed with the free L (Table 4). Furthermore, the Cu^{2+} and Cd^{2+} complexes with L grafted on SBA-15 start to form at lower pHs (Figures 5E and 5F) than those observed with free L. This enhancement in the complex formation constants could also be due to the higher local concentration of metal binding sites on the SBA surface, which is a characteristic feature of ligands grafted on mesoporous materials with high surface areas.

Figure S3 shows the FTIR spectra of the free SBA-15 and the Cu^{2+} and Cd^{2+} complexes with SBA-L. The new bands in the regions 1200–2000 and 3000–4000 cm^{-1} relative to the complex formation, are clearly visible in the spectrum of the Cd^{2+}/SBA-L complex to suggest that the nitrogen atoms are present in the coordination sphere of the metal. The bands between 3000–4000 cm^{-1} can be associated to the presence of water molecules in the metal complex, which form intramolecular bonds. These data agree with potentiometric studies (Figure 5F), which showed that water molecules in the complex dissociate above pH = 8.

SBA-L reuse and metal ions recovery. The adsorption process (4 cycles) of SBA-L towards Cu^{2+} and Cd^{2+} is shown in the Figure 7A, while desorption data (4 cycles) are presented in Figure 7B. To reuse the SBA-L material for the adsorption cycle and recover Cu^{2+} and Cd^{2+} metal ions in the desorption cycle, the solid SBA-L-metal ion obtained from the initial adsorption process were initially suspended in a concentrated EDTA solution. The free SBA-L material was then reused for another adsorption cycle. Figure 7 shows that the copper(II) adsorption capacity of SBA-L exceeded ~ 80% ± 10% (SD) of the original value after four adsorption–desorption processes (Figure 7b), while cadmium(II) adsorption capacity is lowered between second and third cycle from ~ 100% ± 20% (SD) to ~ 60% ± 20% (SD). Of note, after the first adsorption cycle the copper(II) concentration was lowered to 1 ppm (mean value of three independent experiments), while cadmium(II) concentration was decreased to 120 ppb (mean value of three independent experiments). The permissible limit of copper(II) ions in industrial effluents reported by the United State Environmental Protection Agency

(USEPA) is 1.3 mg/L,[45] while according to World Health Organization (WHO) the copper(II) ions content in drinking water should not exceed 2 mg/l.[46-48] The allowable limit for Cd^{2+} in drinking water is 3.0 ppb (WHO).[49] Thus, even low SBA-L quantities (7 mg/L, see Figure 7) could be used for effective copper(II) removal from water, while higher quantities of SBA-L should be used for cadmium(II) removal from drinking water.

Moreover, the ~ 100% ± 4% (SD) recovery of both metals can be obtained with the EDTA treatment and SBA-L can be recycled.

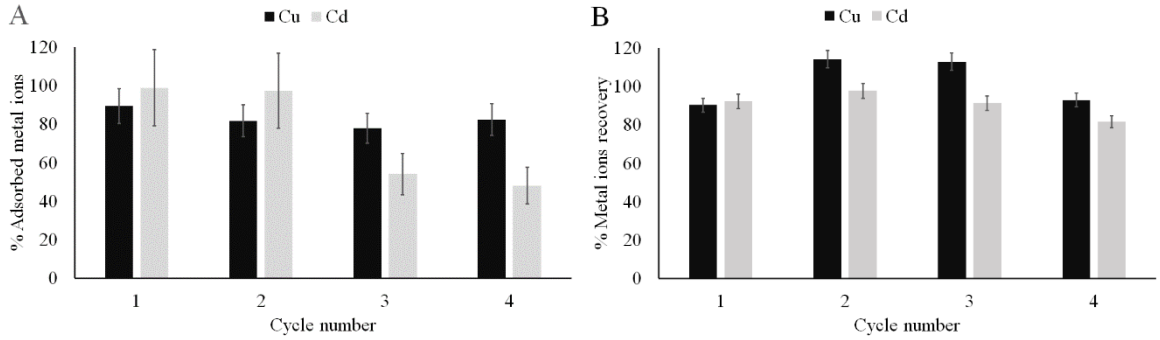

Figure 7. Metal ion recovery study (mean and standard deviation of three independent experiments) with four adsorption (A) – desorption (B) cycles. SBA-L (7 mg mL^{-1}); pH = 7, $[Cu^{2+}]$ = $[Cd^{2+}]$ 10 mg L^{-1}, [EDTA-2Na] = 0.02 mol L^{-1}. Statistical comparison of the samples was performed by one-way ANOVA. P value <0.05 was considered significant.

Conclusions

The fast development of metal-based industries demands new metal-recovery materials, which enables lower metal release into the environment. Grafting efficient-metal chelators on the surface of mesoporous materials is an effective technology that satisfies this requirement. In the present work 2,8-dithia-5-aza-2,6-pyridinophane (L) ligand was grafted on the SBA-15 mesoporous material (internal and external) surface to obtain the highly efficient adsorbent SBA-L. The kinetic studies showed fast Cu^{2+} and Cd^{2+} adsorption (~ 30 min), while adsorption isotherms and potentiometric studies revealed the metal chelation as a unique adsorption mechanism. The adsorption isotherms show an almost complete saturation of adsorbing sites of SBA-L according to a 1:1 stoichiometry between the ligand and the cations in our experimental conditions. This suggests that the adsorbing performance of SBA-L could be modulated by changing the loading of L macrocycle grafted on SBA-15 surface. Moreover, potentiometric studies showed that the formation constants of the metal/ligand complexes (metal = Cu^{2+} and Cd^{2+}) on the mesoporous material surface are higher than those obtained for the complexes formed by free ligand in solution, probably due to the participation of silanols in

the metal coordination core. The chelated metal ions can be efficiently and repeatably removed from the material surface, thus assuring multiple material re-use and metal recovery. The overall results obtained here are promising for the potential use of this type of nanostructured functional material for the adsorption and/or storage, recycle of Cu^{2+} and Cd^{2+} ions from aqueous solutions.

Acknowledgements

Fondazione di Sardegna (FdS) (Progetti Biennali di Ateneo annualità 2018-2019 and 2019-2020) and Regione Sardegna L.R. 7 (CUP: J81G17000150002 and CRP: RASSR79857) are acknowledged for financial support. GRD thanks MIUR PON-RI (DOT1304455) for financing her PhD scholarship.

Conflict of Interest

The authors declare no conflict of interest.

References

1. J. Aaseth, G. Crisponi and O. Anderson, *Chelation therapy in the treatment of metal intoxication*, Academic Press, 2016.
2. A. Luch, *Molecular, Clinical and Environmental Toxicology: Volume 3: Environmental Toxicology*, Springer Science & Business Media, 2012.
3. S. Luckeneder, S. Giljum, A. Schaffartzik, V. Maus and M. Tost, *Global Environmental Change*, 2021, **69**, 102303.
4. G. Sharma, B. Thakur, A. Kumar, S. Sharma, M. Naushad and F. J. Stadler, *Carbohydrate Polymers*, 2020, **241**, 116258.
5. M. Yan, D. Wang, J. Qu, J. Ni and C. W. Chow, *Water research*, 2008, **42**, 2278-2286.
6. H. A. Hasan and M. H. Muhammad, *Journal of Water Process Engineering*, 2020, **33**, 101035.
7. I. L. Calugaru, C. M. Neculita, T. Genty and G. J. Zagury, *Journal of environmental management*, 2018, **212**, 142-159.
8. A. Chatterjee and J. Abraham, *Biotechnology Letters*, 2019, **41**, 319-333.
9. A. Thirunavukkarasu, R. Nithya and R. Sivashankar, *Reviews in Environmental Science and Bio/Technology*, 2020, 1-28.
10. E. M. Usai, M. F. Sini, D. Meloni, V. Solinas and A. Salis, *Microporous and mesoporous materials*, 2013, **179**, 54-62.
11. M. Piras, A. Salis, M. Piludu, D. Steri and M. Monduzzi, *Chemical Communications*, 2011, **47**, 7338-7340.
12. C. Vittoni, G. Gatti, I. Braschi, E. Buscaroli, G. Golemme, L. Marchese and C. Bisio, *Materials*, 2020, **13**, 2690.
13. G. Kickelbick, *Angewandte Chemie International Edition*, 2004, **43**, 3102-3104.
14. W. Li and D. Zhao, *Chemical Communications*, 2013, **49**, 943-946.
15. B. Szczęśniak, J. Choma and M. Jaroniec, *Chemical Communications*, 2020, **56**, 7836-7848.
16. J. I. Lachowicz, A. H. Emwas, G. R. Delpiano, A. Salis, M. Piludu, L. Jaremko and M. Jaremko, *Advanced Materials Interfaces*, 2020, **7**, 2000544.
17. P. Duenas-Ramirez, C. Bertagnolli, R. Müller, K. Sartori, A. Boos, M. Elhabiri, S. Bégin-Colin and D. Mertz, *Journal of Colloid and Interface Science*, 2020, **579**, 140-151.

18. M. Laprise-Pelletier, M. Bouchoucha, J. Lagueux, P. Chevallier, R. Lecomte, Y. Gossuin, F. Kleitz and M.-A. Fortin, *Journal of Materials Chemistry B*, 2015, **3**, 748-758.
19. A. M. Sacara, V. Nairi, A. Salis, G. L. Turdean and L. M. Muresan, *Electroanalysis*, 2017, **29**, 2602-2609.
20. A.-M. Sacara, F. Pitzalis, A. Salis, G. L. Turdean and L. M. Muresan, *ACS Omega*, 2019, **4**, 1410-1415.
21. N. Cotolan, L. M. Mureşan, A. Salis, L. Barbu-Tudoran and G. L. Turdean, *Water, Air, & Soil Pollution*, 2020, **231**, 1-8.
22. A. D. Zubenko and O. A. Fedorova, *Russian Chemical Reviews*, 2020, **89**, 750.
23. B.-L. Su, X.-C. Ma, F. Xu, L.-H. Chen, Z.-Y. Fu, N. Moniotte, S. B. Maamar, R. Lamartine and F. Vocanson, *Journal of Colloid and Interface Science*, 2011, **360**, 86-92.
24. M. Sperling, X.-p. Yan and B. Welz, *Spectrochimica Acta Part B: Atomic Spectroscopy*, 1996, **51**, 1875-1889.
25. A. G. Algarra, M. G. Basallote, R. Belda, S. Blasco, C. E. Castillo, J. M. Llinares, E. García-España, L. Gil, M. Á. Máñez and C. Soriano, *Journal*, 2009.
26. A. J. Blake, A. Bencini, C. Caltagirone, G. De Filippo, L. S. Dolci, A. Garau, F. Isaia, V. Lippolis, P. Mariani and L. Prodi, *Dalton Transactions*, 2004, 2771-2779.
27. A. Albert and E. P. Serjant, Chapman and Hall, London, 1984 (Chapter 2).
28. J. I. Lachowicz, G. R. Delpiano, D. Zanda, M. Piludu, E. Sanjust, M. Monduzzi and A. Salis, *Journal of Environmental Chemical Engineering*, 2019, **7**, 103205.
29. I.-C. Apat, *Manuali e linee guida*, 2003, **29**, 2003.
30. L. Alderighi, P. Gans, A. Ienco, D. Peters, A. Sabatini and A. Vacca, *Coordination Chemistry Reviews*, 1999, **184**, 311-318.
31. E. P. Barrett, L. G. Joyner and P. P. Halenda, *Journal of the American Chemical Society*, 1951, **73**, 373-380.
32. C. Baes Jr and R. Mesmer, *Jon Wiley & Sons: New York*, 1976.
33. L. N. Nemeş and L. Bulgariu, *Open Chemistry*, 2016, **14**, 175-187.
34. E. Da'na, N. De Silva and A. Sayari, *Chemical Engineering Journal*, 2011, **166**, 454-459.
35. E. C. Lima, A. Hosseini-Bandegharaei, J. C. Moreno-Piraján and I. Anastopoulos, *Journal of Molecular Liquids*, 2019, **273**, 425-434.
36. I. D. Mall, V. C. Srivastava, N. K. Agarwal and I. M. Mishra, *Chemosphere*, 2005, **61**, 492-501.
37. N. Dyatlova, V. Y. Temkina and K. Popov, 1988 Moscow: Khimiya. Ed. Ovsyannikova, 544.
38. R. E. Mewis and S. J. Archibald, *Coordination Chemistry Reviews*, 2010, **254**, 1686-1712.
39. P. Antunes, P. M. Campello, R. Delgado, M. G. Drew, V. Félix and I. Santos, *Dalton Transactions*, 2003, 1852-1860.
40. J. Costa and R. Delgado, *Inorganic Chemistry*, 1993, **32**, 5257-5265.
41. C. Caltagirone, A. Bencini, F. Demartin, F. A. Devillanova, A. Garau, F. Isaia, V. Lippolis, P. Mariani, U. Papke and L. Tei, *Dalton Transactions*, 2003, 901-909.
42. A. Casale, A. De Robertis and F. Licastro, *Thermochimica acta*, 1989, **143**, 289-298.
43. M. Kodera, T. Kita, I. Miura, N. Nakayama, T. Kawata, K. Kano and S. Hirota, *Journal of the American Chemical Society*, 2001, **123**, 7715-7716.
44. B. Chen, H. Yao, W. Huang, P. Chattopadhyay, J. Lo and T. Lu, *Solid state sciences*, 1999, **1**, 119-131.
45. https://www.epa.gov/dwreginfo/lead-and-copper-rule.
46. H. Aydın, Y. Bulut and Ç. Yerlikaya, *Journal of environmental management*, 2008, **87**, 37-45.
47. E.-S. El-Ashtoukhy, N. K. Amin and O. Abdelwahab, *Desalination*, 2008, **223**, 162-173.
48. E. Eren, *Journal of hazardous materials*, 2008, **159**, 235-244.
49. WHO, "Guidelines for the safe use of wastewater, excreta and greywater," World Health Organization, vol. I, p. 95, 2006.